Int. J. Electrochem. Sci., 13 **(2018)** 3356 – 3371, doi: 10.20964/2018.04.06

International Journal of
ELECTROCHEMICAL
SCIENCE
www.electrochemsci.org

Isolation of Microcrystalline Cellulose (MCC) from Oil Palm Frond as Potential Natural Filler for PVA-$LiClO_4$ Polymer Electrolyte

M. Hazwan Hussin[1,*], *Nurhanina Ayu Husin*[1], *Ibrahim Bello*[1], *Nurmaizatulhana Othman*[1], *Mohamad Abu Bakar*[1], *M.K. Mohamad Haafiz*[2]

[1] Materials Technology Research Group (MaTReC), School of Chemical Sciences, Universiti Sains Malaysia, 11800 Minden, Penang, Malaysia.
[2] School of Industrial Technology, Universiti Sains Malaysia, 11800 Minden, Penang, Malaysia.
[*]E-mail: mhh@usm.my; mhh.usm@gmail.com

Received: 6 December 2017 / *Accepted:* 22 January 2018 / *Published:* 6 March 2018

In this study, microcrystalline cellulose (MCC) was extracted from organosolv oil palm fronds (OPF) pulp *via* acid hydrolysis method. The isolated OPF-MCC were characterized using complementary analysis such as FTIR, CP/MAS ^{13}C NMR, XRD, GPC, TGA, DSC, SEM and N_2-BET. It was found that the isolated OPFMCC was identified as cellulose type I polymorph with high crystallinity index than α-cellulose ($CrI_{OPF\ MCC}$: 76.38 % > $CrI_{\alpha\text{-cellulose}}$: 73.37 %). The obtained OPFMCC was then incorporated with PVA-$LiClO_4$ at different $LiClO_4$ loading (0, 5, 10, 15, 20 %) through solution casting technique to produce biodegradable polymer electrolytes of OPFMCC-PVA-$LiClO_4$. The fabricated films were further analyzed using electrochemical impedance spectroscopy (EIS) and cyclic voltammetry (CV). It interesting to note that, a maximum conductivity was found to be 1.88×10^{-4} S cm^{-1} for OPF MCC-PVA-20 % $LiClO_4$ with electrochemical stability window potential around 1.9 V.

Keywords: Oil palm frond; microcrystalline cellulose; polymer electrolytes.

1. INTRODUCTION

Solid polymer electrolyte (SPE) has a great potential in view of its applications in electrochemical devices such as fuel cells, sensors, high energy densities and electronic devices [1]. The SPE have been discovered useful to replace conventional liquid electrolytes [2]. (SPE) conduct protons from the anode to the cathode while insulating the electrodes electrically. High ionic conductivity (SPE) has long been desired for the next generation as an alternative for the high energy and safe rechargeable lithium batteries [3].

Previous study have been reported that by using different type of filler incorporated with different types of polymer matrix such as poly (ethylene oxide), PEO, poly(acrylonitrile), PAN, poly(methyl methacrylate), PMMA and copolymer poly(vinylidene fluoride-hexafluoro propylene), PVdF-HFP [4]. poly(vinyl alcohol) PVA however, is a favourable polymer due to its high end application such as sensors, in bio-medical fields, blood prosthetic devices, electric double layer capacitor and electrochromic windows [5]. PVA has been a perfect polymer due to its excellent film forming capability, excellent mechanical strength, bio-compatibility, electrochemical stability, high tensile strength and resistance [1]. Blending the PVA with other polymer like cellulose is favourable as it performed higher polar hydroxyl group that promotes the localized stability in the solid polymer structure [6]. The polymer blend with $LiClO_4$ salt will increase the amorphicity and conducing ionic species in the polymer membrane [3].

Cellulose (Fig.1), is a natural polysaccharide polymer that contains 3000 or more glucose units that join together to form a long chain which is linked by β - 1, 4 glycoside bonds [7]. It is composed of four different types of polymorphous form such as cellulose I, II, III and IV. Cellulose I is the most widespread crystalline form, which consists of an assembly succession of crystallites and disordered amorphous regions [8]. The natural crystal is made up of metastable cellulose I with all cellulose strands in a highly ordered parallel arrangement [9]. In addition, it possesses higher molecular weight, crystalline structure and insoluble in water [10].

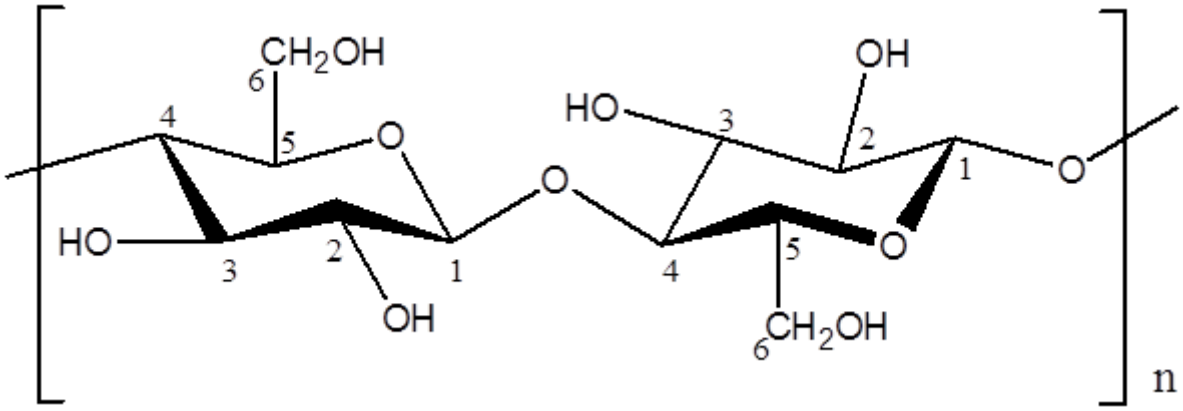

Figure 1. The chemical structure of cellulose

Meanwhile, microcrystalline cellulose (MCC) is a fine, white crystalline, biodegradable material which is odourless [11]. The isolation of MCC from alpha cellulose can be performed by different processes such as reactive extrusion, enzyme mediated, steam explosion and acid hydrolysis [12]. various sources of cellulose and isolation method affect the molecular weight, particle size, crystallinity, surface area, moisture content and porous structure of extracted MCC [13]. Due to its high sorption, absence of toxicity, chemical inactivity and its great hygroscopicity, MCC has great potential in pharmaceutical industries, as water retainer in medical industries, as stabilizer and emulsifier in several dairy compounds and as dye adsorbent for waste water treatment [14-18]. MCC can be derived from many types of cellulose sources such as cotton, wood, cereal straw, bagasse and

corn cob, bamboo, sugar beet pulp, luffa cylindrical, orange mesocarps, jute, rice and bean hulls, hemps stalks and rice husks, newsprint as well as oil palm frond [13].

The oil palm frond (OPF) has been discovered as a future alternative of biodegradable, sustainable and renewable raw material. In Malaysia alone, the oil palm frond is abundant throughout the year and it was estimated that around 26 million metric tonnes of oil palm fronds were produced annually [19]. It was revealed that the approximate composition of the OPF (% w/w) is cellulose 35.73 ± 1.34 %, hemicelluloses 28.39 ± 1.34 % and Klason lignin 24.62 ± 1.17 % on a dry weight basis [20]. Recent studies have shown the applicability of OPF as livestock feed, adsorbent, source of sugar, biofuel and corrosion inhibitor [21-26]. Despite of its potential application, there is no comprehensive study on the utilization of microcrystalline cellulose from OPF as biodegradable filler in solid polymer electrolyte.

Therefore, the scope of the present work is to study the physicochemical and ionic conductivity of OPF MCC-PVA-$LiClO_4$ as a potential biodegradable polymer electrolyte. The MCC was isolated from OPF pulp *via* acid hydrolysis. The isolated OPF MCC were characterized by using the Fourier Transform Infrared Spectroscopy (FTIR), cross polarization magic angle spinning nuclear magnetic resonance (CP/MAS ^{13}C NMR) and X-ray diffraction (XRD) spectroscopy, gel permeation chromatography (GPC), thermal behaviour and N_2 adsorption of Brunaeur-Emmett-Teller (BET). Different ratio of MCC-PVA-$LiClO_4$ polymer electrolyte was prepared by solution casting technique. The ionic conductivity of the prepared polymer electrolyte were evaluated using electrochemical methods via electrochemical impedance spectroscopy (EIS) and cyclic voltammetry (CV). Understanding the ionic conductivity of MCC-PVA-$LiClO_4$ can help its further application especially in electronic devices.

2. MATERIALS AND METHODS

2.1 Materials

The oil palm fronds (OPF) were collected from Ladang Transkrian, near Nibong Tebal, Pulau Pinang. The strands were cut into small pieces. It was sun dried for 3 days before grinded with Wiley mill into fine powder. The ground OPF was dried in an oven at 50 ˚C for 24 h. The ground OPF was first subjected to Soxhlet extraction with an ethanol-toluene (2:1) mixture in a Soxhlet apparatus for 5 h at 50 ˚C [14]. The preliminary proximate analysis of the OPF (% w/w) was found to have hemicelluloses 17.5 ± 3.7 %, cellulose 45.2 ± 5.3 %, extractives 6.6 ± 1.3 %, moisture content 4.8 ± 0.2 %, ash content 3.6 ± 0.2 % and Klason lignin 22.2 ± 2.3 % on a dry weight basis.

2.2 Organosolv pulping

The organosolv pulping process was carried out in a 0.6 L steel reactor. The conditions were outlined by Hussin et al. [20] with slight modifications. The organosolv pulping condition was OPF biomass to organic solvent, 1: 8 ratio by using 65 % (w/w) aqueous ethanol with 0.5 % (w/v) of 4 N

H_2SO_4 as catalyst. The pressure for the organosolv pulping was around 25 bar. The cooking times that are favourable in this method was set 1 h under controlled temperature of 190 ˚C [27]. The pulp was filtered using vacuum filtration before drying in an oven at 50 ˚C for 24 h.

2.3 Pulp bleaching

The bleaching process of the resulting pulp was performed for the production of holocellulose. The purpose of the bleaching process is to enhance the physical and optical qualities (whiteness and brightness) of the pulp by removing or decolorizing the remaining lignin. The bleaching of chemical pulp was carried out with sodium chlorite without degrading the cellulose. The holocellulose was isolated from the pulp by treating the pulp with a mixture of acetic acid and sodium chlorite. Around 4.5 g of the pulp was placed in 125 mL deionized water with the addition of 3.0 mL of glacial acetic acid and 3.0 g sodium chlorite was heated for 2 h at 70 ˚C with constant stirring [28]. The holocellulose was filtered and washed with excess of distilled water. The resulted holocellulose was dried in an oven at 50 ˚C for 24 h.

2.4 Mercerization and acid hydrolysis

The dried holocellulose sample, (2.0 g) was treated with 100 mL of 10 % (w/v) of NaOH for 30 min. Next, around 100 mL of distilled water was added and the resulting slurry was stirred for another 30 min at room temperature. The resulting α-cellulose was filtered, washed immediately with 1% (w/v) HOAc, 5 % (w/v) NaOH with the excess of distilled water and then dried in an oven at 50 ˚C for 24 h.

OPF microcrystalline cellulose (OPF MCC) was produced by using the method as describe by Chauchan et al. [12] with slight modification. The α-cellulose obtained from the mercerization method was further treated with 2 M of HCl at 80 ˚C for 1 h with the ratio of solid to liquor (1:30, w/v) was applied. The reaction mixture was further filtered and washed with distilled water, followed by 5 % (w/v) NaOH and excess of distilled water. The OPF MCC was dried in an oven at 50 ˚C and later ground by using mortar until fine powder was obtained.

2.5 Preparation of the polymer electrolyte

The composite film of polymer electrolyte was prepared by using the solution casting method. The film was prepared according to Sudhakar et al. [29] with slight modification. Known quantity of PVA and OPF MCC (1.0 g as filler) were added with weight ratio of 80:20 in 100 mL of distilled water and vigorously stirred until homogeneous for 2 h at 70 ˚C. After 2 h, the mixture was further added with 1.0 g of OPF MCC (20 % wt) as filler, 1.0 g glycerol as chelating agent and different percentage of lithium perchlorate, $LiClO_4$ (0, 5, 10, 15, 20 % wt; simplified as S1-S5). The mixture was blend while continuously stirring for 3 h at 100 ˚C until the solution formed a highly viscous solution. The viscous solution were cast onto a petri dish and cover with aluminium foil. The dishes

were further dried in an oven at 50 ˚C for 72 h. The solid film was peeled from the petri dish and the thickness of solid film was measured using the Vernier Caliper Gauge with an accuracy of 0.001 mm.

2.6 Characterization

2.6.1 FTIR analysis

Fourier Transform Infrared Spectroscopy (FTIR) spectra of α-cellulose, OPF MCC and commercial MCC were carried out by Perkin-Elmer System 2000 spectrometer using the KBr method with 1:20 ratio. The spectra were recorded in the range of 4000-400 cm^{-1}, with resolution of 4.0 cm^{-1}, and the spectra were recorded for 20 scans per sample.

2.6.2 CP/MAS ^{13}C NMR analysis

The solid state nuclear magnetic resonance employing the technique of cross-polarization magic angle spinning (CP/MAS) experiments were carried out by using Bruke Avance 400 MHz spectrometer, operating at a frequency of 76.46 MHz. The spectra were recorded for 10 000 scans per sample. The samples were pressed into cylindrical zirconia rotors and spun at magic angle at 7 kHz.

2.6.3 XRD analysis

X-ray diffraction (XRD) analysis was performed by using a PANalytical X'Pert PRO MRD PW 3040. The diffraction patterns were recorded using Cu-Kα radiation at 40 kV and 40 mA. The α-cellulose, OPF MCC and commercial MCC were compressed under a pressure of 50 MPa [30] to become a pellet with 25 mm in diameter. The crystallinity index, *CrI* was calculated using the Eq.1 as outlined by Hussin et al. [18]

$$\%\ CrI = \frac{I_{002} - I_{am}}{I_{002}} \times 100 \qquad \text{(Eq.1)}$$

Where *CrI* is crystallinity index, I_{002} is the peak intensity of the 002 latice plane at about 2θ = 22.0˚ and I_{am} is the peak intensity of the amorphous phase which correspond to the peak at about 2θ = 18.0˚ for cellulose type I.

2.6.4 GPC analysis

The sample of α-cellulose, OPF MCC and commercial MCC were derivatized using the phenyl isocynate to obtain cellulose tricarbanilate, (CTC) precipitation. This process was described by Foston [31] and the detail as followed: 15 mg of the dried α-cellulose and MCC samples, placed in 25 mL flask was treated with 4mL anhydrous pyridine and 0.5 mL phenyl isocyanate, sealed with Teflon-lined cap. The reaction mixture was then kept in an oil bath at 70 ˚C and allowed to stir for 48 h. After the reaction, the solution was cooled and 1 mL methanol was added to quench any remaining phenyl isocynate. Subsequently, the mixture was poured into 100 mL methanol-water (7:3). The precipitated

CTC was purified through centrifuging by repeated washing with methanol-water for three times, and water two times. The CTC was lyophilized. The average molecular weight (M_n) and weight (M_w) of cellulose were determined after derivatization by GPC with Waters 1525 Binary HPLC Pump consisting of refractive index, RI detector using tetrahydrofuran as eluent. Standard polystyrene samples which is monodisperse polymer standards were used to construct a calibration curve. Data were collected and analyzed with a Waters Breeze System software. The apparent average-number, DP_n and average-weight, DP_w were calculated by dividing respectively M_n and M_w values by 519, the monomer equivalent weight of CTC.

2.6.5 Thermal behavior

Thermal gravimetric analysis of α-cellulose, OPF MCC and commercial MCC were performed at a scanning rate of 10 ˚C min^{-1} by using a thermogravimetric analyzer Perkin-Elmer TGA 7. The samples were heated from 30 to 900 ˚C and held for 5 min at 900 ˚C. Differential scanning calorimeter (DSC) thermograms were obtained using a Perkin Elmer Pyris 1' DSC which was heated from 30 to 400 ˚C at heating rate of 10 ˚C min^{-1}. Second heating data was used for analysis.

2.6.6 Surface area analysis

The BET surface area, external surface area, total pore volume and pore size of the studied samples were obtained by analyzing the sample using a Quantachrome Nova Win2© 1994-2002

2.6.7 Electrochemical studies

Ionic conductivity of the prepared film was measured using HIOKI 3522-50 LCR HiTester impedance unit. The AC frequency was scanned from 1 MHz to 1 Hz at 10 mV amplitude. The prepared sample was placed between the stainless steel electrodes. The resulting data was fitted to an equivalent circuit using Zsim Demo software. The ionic conductivity, σ was calculated using formula below:

$$\sigma = \frac{L}{R_b A} \quad \text{(Eq.2)}$$

Where L is the thickness of the film (in cm), R_b is the bulk resistance of the polymer electrolyte (Ω cm^2) and A is the expose area of the polymer electrolyte (4.9087 cm^2).

The electrochemical window stability was acquired in order to investigate the electrochemical stability of the solid polymer electrolyte. In this test, cyclic voltammetry analysis was performed by using a BASi Epsilon-EC potentiostat, where the polymer electrolyte film was placed between two stainless steel electrodes. The parameters were set to have a voltage at -1.5 V to +1.5 V with a scan rate of 10 mV s^{-1}.

3. RESULTS AND DISCUSSION

3.1 FTIR analysis

FTIR spectroscopy has proven to be a valuable tool for determining the functional group thus leading to the prediction of the structure of the sample. FTIR spectra of α-cellulose, OPF MCC and commercial MCC samples are shown in Fig. 2. FTIR spectroscopy revealed the similarities between all spectra which an indication that all sample have almost similar in chemical composition. It is similar to that of pure cellulose as reported elsewhere [11,14,32]. The broad absorption band located around 3300 to 3500 cm^{-1} was due to stretching of the –OH groups and the absorption from 2800 to 3000 cm^{-1} was referred to CH_2 groups [33]. Besides, the absorption band around 1646 cm^{-1} in the samples indicated the bending of water molecules due to the strong interaction between cellulose and water [34]. The band corresponded to a symmetric CH_2 bendings at 1431 cm^{-1} increased in both OPF MCC and commercial MCC as compared to α-cellulose This band is known as the crystalillinity band [35], where increase in the intensity demonstrates higher degree of crystallinity. Meanwhile, the absorption band around 1163 to 1200 cm^{-1} indicates the C–O–C stretching and the peak around 895 to 900 cm^{-1} were associated to C–H rock vibration of cellulose (anoumeric vibration of β-glucosides) observed in OPF MCC samples [36]. In addition, the presence of a peak at 801 cm^{-1} in the OPFMCC and commercial MCC spectra was referred as C–H bending and puckering ring of arenes.

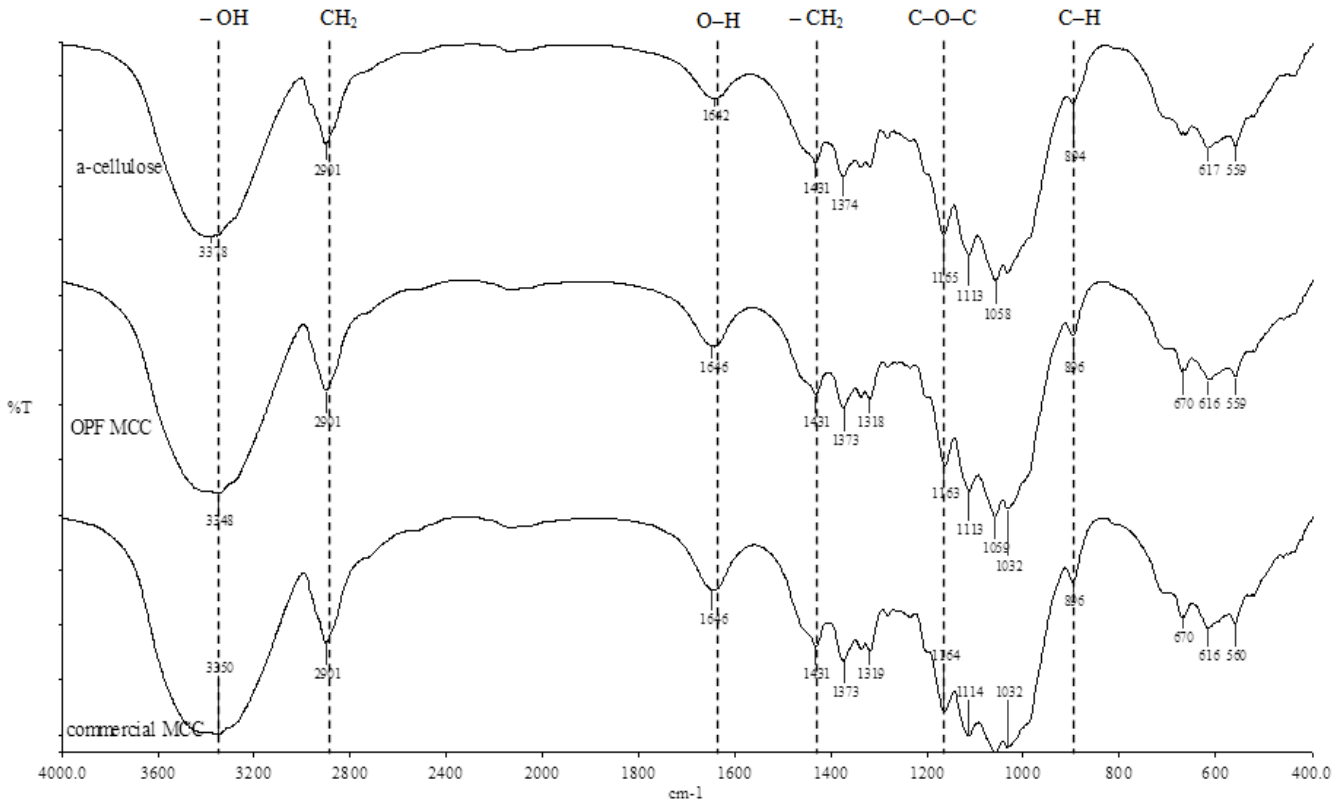

Figure 2. The FTIR spectra of α-cellulose, OPF MCC and commercial MCC

Interestingly, the absence of peaks located in the range of 1509 to 1609 cm^{-1} corresponds to C=C aromatic skeletal vibration, indicate the complete removal of lignin [33,37]. The absence in the region of 1700 to 1740 cm^{-1} which corresponds to either acetyl or uronic ester groups of hemicelluloses has proved that the hemicelluloses were removed during the acid hydrolysis [38]. It can be concluded that the organosolv pulping and bleaching technique used able to remove non-cellulosic material in OPF and leave behind the pure cellulose.

3.2 CP/MAS ^{13}C NMR analysis

Solid state CP/MAS ^{13}C NMR spectra of the OPF MCC samples prepared from organosolv OPF pulp as well as commercial MCC are shown in Fig. 3. Peaks have been assigned based on the literature and are displayed on the spectra [31,39]. Peaks in the region between 59 to 106 ppm were due to the different carbon in the cellulose structure.

In NMR spectra of both MCC samples, the resonance lines were assigned to carbon of C1 (104,106 ppm) and a cluster of resonances at 70-75 ppm belonging to the C2, C3 and C5 carbons [40]. The expected C6 peaks at approximately around 65-69 ppm were well resolved. In addition, the C6 peaks located in the regions of 62 – 64 ppm corresponds to the amorphous region. The signals from 86 to 92 ppm were referred to C4 carbon from crystalline forms together with paracrystalline regions. The broader up field resonances in the region of 80 to 86 ppm indicates the amorphous region. The similarities for the findings of the spectra of cellulose derivatives were reported by Trache et al. [14].

3.3 Molecular weight distribution of cellulose samples

The M_w, M_n and polydispersity (M_w/M_n) of OPF α-cellulose, OPF MCC and commercial MCC are summarized in Table 1. From Table 1, the reduction in molecular weight clearly occurred, this due to the depolymerisation of cellulose through cleavage of glycosidic bonds. It was clearly observed that the OPF MCC produce lower values of polymerization and polydispersity. This proves that the acid hydrolysis treatment induced to form smaller fragments of cellulose [18]. Moreover, it was found that the OPF MCC produce lower molecular weight compared to that of OPF α-cellulose and commercial MCC.

Table 1. Parameters obtained from the GPC analysis for the sample studied.

Sample	M_n (g mol^{-1})	M_w (g mol^{-1})	DPI	DP_n	DP_w
α-cellulose	442	31137	70.44	0.85	59.99
OPF MCC	7221	11824	1.64	13.91	22.78
Commercial MCC	9457	17237	1.83	18.22	33.21

Average number of molecular weight, M_n ; Average weight of molecular weight, M_w ; Polydispersity index, DPI ; Average number of degree polymerization, DP_n ; Average weight of degree polymerization, DP_w.

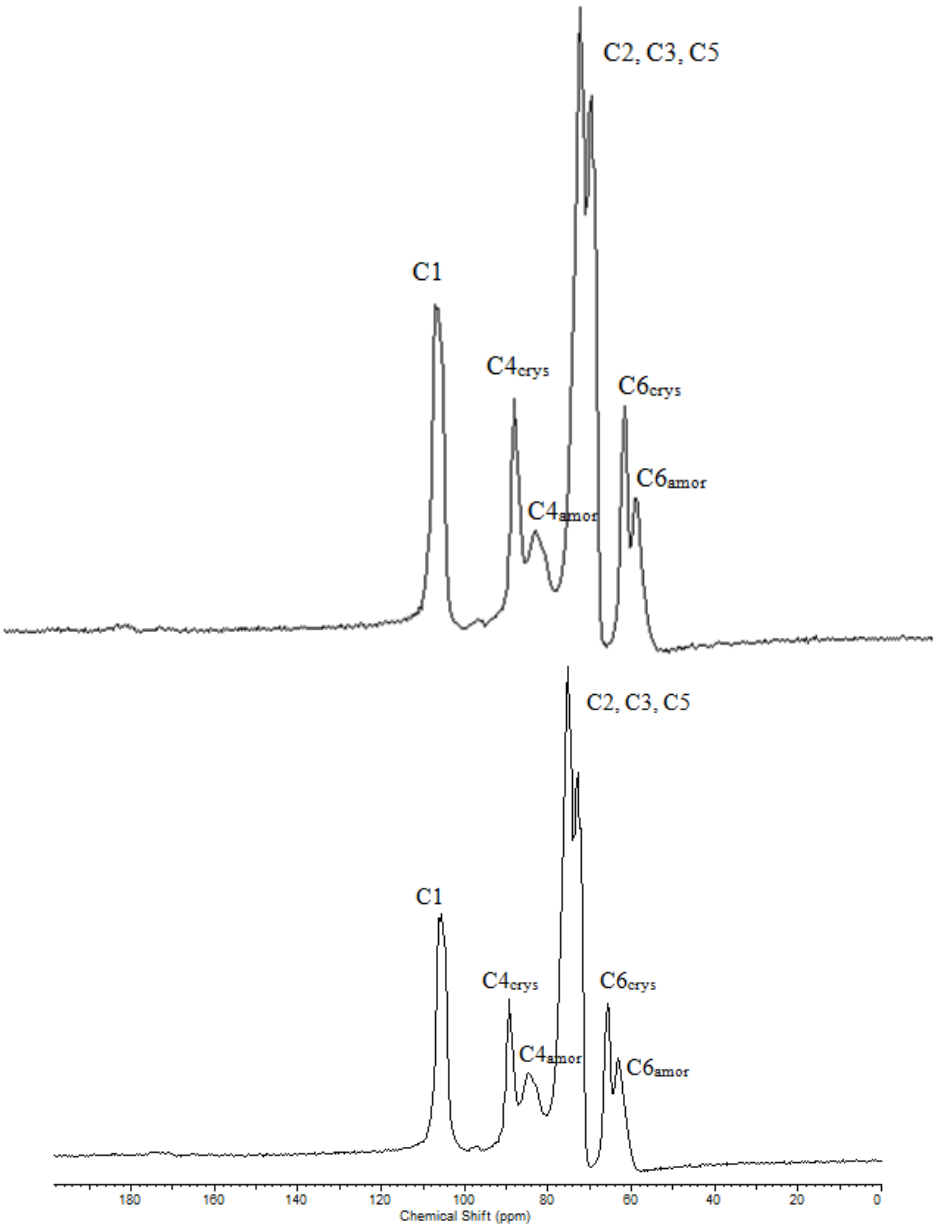

Figure 3. The solid state CP/MAS ^{13}C NMR spectra of OPF MCC and commercial MCC

3.4 XRD analysis

The X-ray diffraction patterns of α-cellulose, OPF MCC and commercial MCC samples are displayed in Fig. 4. The crystallinity indexes of the different samples are given in Table 2. The diffraction pattern typical of Cellulose I show diffraction peaks of 2θ angles at 18.0˚ and 22.0˚. This indicates that the MCC sample obtained from OPF were made up of cellulose type I (22.0˚, 002 lattices). This phenomenon could be due to the mixing of the raw material to the low concentration of sodium hydroxide solution (10 % NaOH) with the short time exposure. Similar observation has been reported earlier by Gupta et al. [41].

It was clear that the diffraction peak of both MCC located at 22.0˚ becomes sharper and it corresponds to the increases in crystallinity. After acid hydrolysis treatment of α-cellulose, the

crystallinity index of OPF MCC was increased to 76.38 %. These revealed that after acid hydrolysis treatment, the residual hemicellulose in α-cellulose (which is more amorphous) was mostly dissolved and lignin-hemicellulose-cellulose interactions were also disrupted, which later released the individual crystallinites [14,36]. All XRD diffraction data were highly crystalline native cellulose I without the existence of cellulose II. In addition, acid hydrolysis treatment is helpful to obtain the higher purity cellulose without cellulose degradation [14].

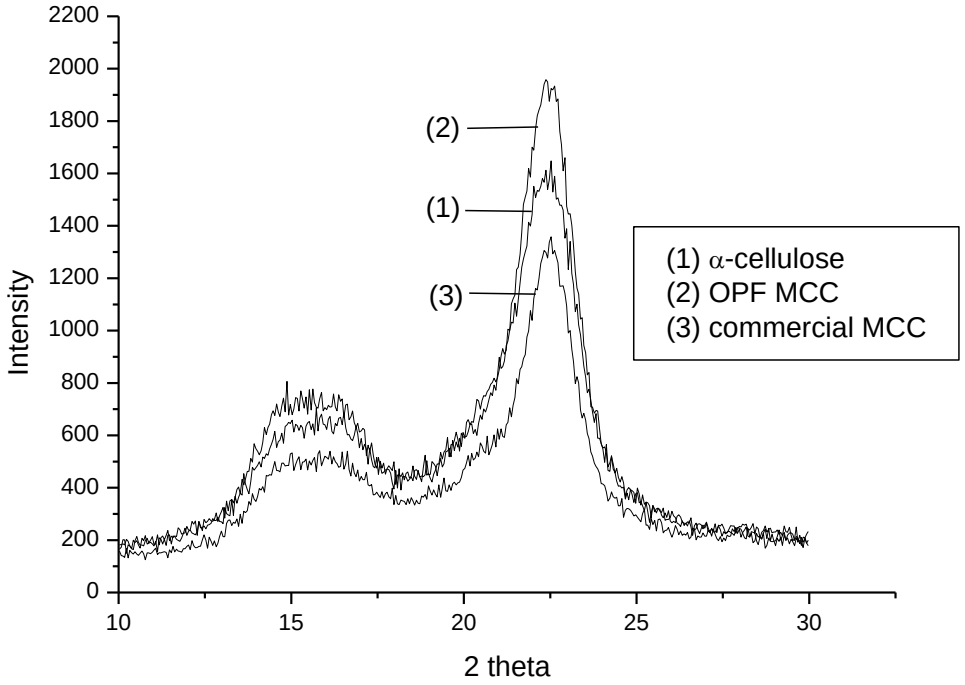

Figure 4. X-ray diffraction pattern of α-cellulose, OPF MCC and commercial MCC

Table 2. Crystallinity index, *CrI (%)* of α-cellulose, OPF MCC and commercial MCC

Sample	Lattice plane, I_{002}	Amorphous phase, I_{am}	Crystalinity index,*CrI (%)*
α-cellulose	1551	413	73.37
OPF MCC	1689	399	76.38
Commercial MCC	1306	358	72.59

3.5 Thermal analyses of cellulose

Thermal stability were obtained by identifying the weight loss of the sample after heating over the high temperature using Thermal gravimetry analyzer (TGA) and derivative thermograms (DTG). The TGA curves are depicted in Fig. 5. The TGA curves show two weight loss stages in the region of 30-900 ˚C. Based on Fig. 5, the first degradation stages at around 60-100 ˚C was due to the removal of

water within the cellulosic material. Meanwhile, the major degradation at around 250-450 ˚C was due to the degradation of cellulose whereby decomposition of glycosyl units occur followed by its conversion to char. It was believed that after acid hydrolysis treatment, the OPF MCC was expected to have a higher weight loss, perhaps due to the high purity of microcrystal-sized cellulose which corroborates higher thermal stability [11].

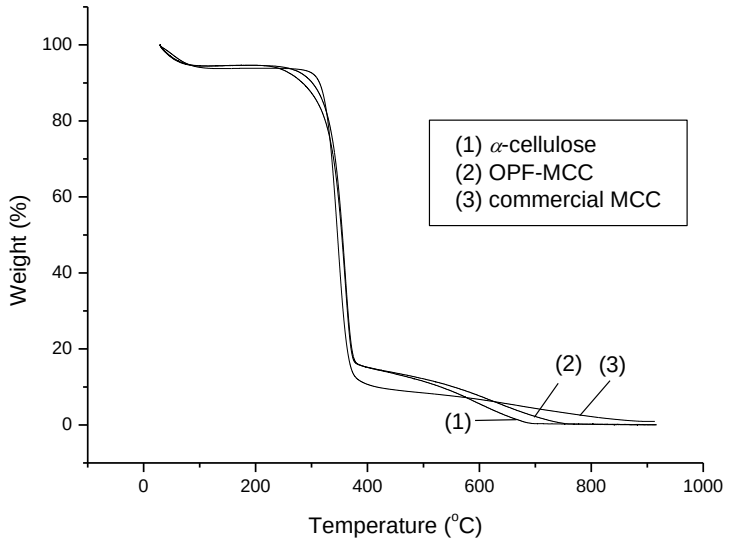

Figure 5. The TGA thermograms of α-cellulose, OPF MCC and commercial MCC

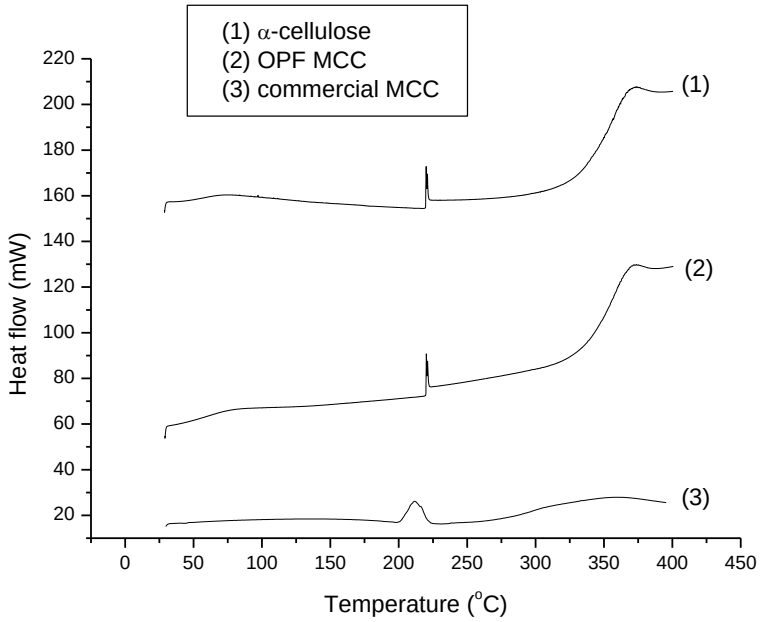

Figure 6. The Differential Scanning Calorimeter (DSC) thermograms of α-cellulose, OPF MCC and commercial MCC

From the DSC analysis as Fig. 6, it is shown that the melting temperature (T_m) for OPF MCC and α-cellulose perform at higher level due to the elimination of hemicelluloses after acid hydrolysis treatment. The value of T_m for OPF MCC and commercial MCC were 220.19 ˚C and 211.58 ˚C

respectively. The higher onset temperatures were often related to higher thermal stability. According to this result, it shows that the OPF MCC samples possesses high thermal stability and will be suitable for applications such as biocomposites, pharmaceutical compounds and food stabilizers [14].

3.6 BET surface analysis

Adsorption of N_2 at subcritical temperatures (BET) is an advanced technique for the determination of the specific surface area of dispersed solids [42]. The BET surface area, total pore volume, cumulative volume of pores and average pore width obtained from the ground OPF, OPF MCC and commercial MCC are shown in Table 3. After acid hydrolysis treatment, a better improvement in the BET surface of the OPF MCC sample was observed as compare to the commercial MCC and ground OPF. Based on the average pore width, the OPF MCC (2.02 nm) can be classified as micropores while both α-cellulose (4.05 nm) and commercial MCC (3.45 nm) can be classified as mesopores, respectively. The BET surface area of disperse, nonporous or macroporous materials pore diameter is >50 nm, mesoporous materials with pore diameter between 2.5 to 50 nm and the microporous materials around <2.5 nm.

Table 3. Characteristics of OPF, OPF MCC & commercial MCC obtained by BET Analysis

Sample	BET surface area ($m^2\ g^{-1}$)	Total pore volume ($cm^3\ g^{-1}$)	Cumulative pore volume ($cm^3\ g^{-1}$)	Average pore width (nm)
OPF	2.04	3.61	0.0022	4.05
OPF MCC	10.10	0.0051	0.0041	2.02
Commercial MCC	4.47	0.0038	0.0038	3.45

3.7 Electrochemical studies of OPFMCC-PVA-$LiClO_4$ polymer electrolyte.

One of the most important parameter for polymer electrolyte is their bulk ionic conductivity, σ. The extrapolation of EIS data was done by fitting it with an equivalent electrical circuit (Fig. 7). The bulk ionic conductivity of the prepared film can be obtained from the complex impedance spectra of polymer electrolyte containing a film OPF MCC-PVA-$LiClO_4$ as shown in Fig. 8. The ionic conductivity values of the polymer electrolyte are summarized in Table 4. From the Table 4, it was observed that as the concentration of $LiClO_4$ salt increases from 0 to 20 wt. %, the ionic conductivity for polymer electrolytes were also increased. This could be due to the increase in the number of charge carriers in the polymer electrolyte system. Besides, the ionic conductivity also depends on the mobility along with polymer segmental mobility or the polymer chain mobility [4]. The lithium ions are the most probable species for carrying charges in polymer electrolytes and it is clear that the conductivity are corresponds to the present of Li^+ ions [1]. Obviously, the maximum ionic conductivity was found to be 1.88×10^{-4} S cm^{-1} for S5 (OPF MCC-PVA-20 % $LiClO_4$) film. The higher conductivity of S5

film could be due to the properties of OPF MCC filler which related to the low molecular weight, high porosity and the high degree of crystallinity that promotes better ion transport. In addition, the comparison in terms of the ionic conductivity value between the current research with the previous work done by Rathod et al. [43] has evidence that OPF MCC provides higher conductivity to than of modified cellulose.

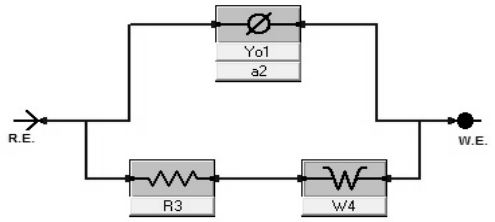

Figure 7. An equivalent electrical circuit used for electrochemical impedance spectroscopy (EIS) fitting

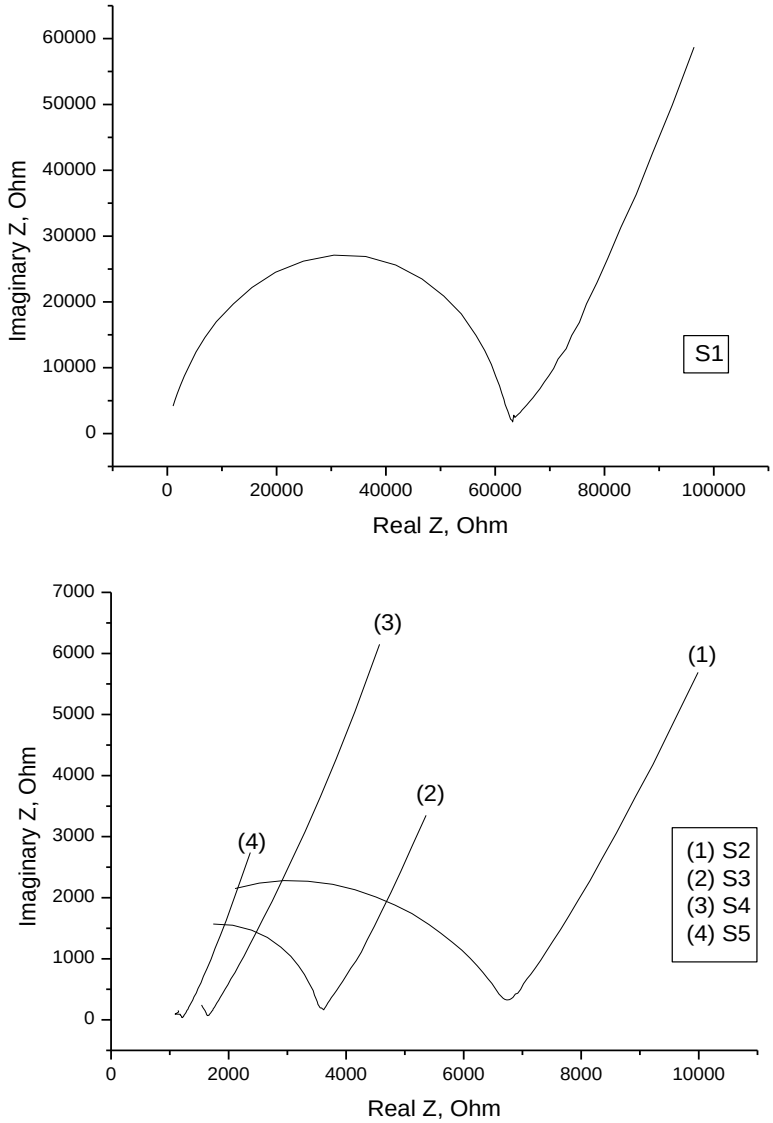

Figure 8. Nyquist plots of 0 % of $LiClO_4$ (above) in organosolv MCC-PVA and different percentage (5, 10, 15, 20 % wt) of $LiClO_4$ in organosolv MCC-PVA (below)

Cyclic voltammetry (CV) is a simple and good method to estimate the working voltage range of the polymer electrolytes. This test is one of the important and necessary parameter for further application in electrochemical devices especially for the batteries. Fig. 9 shows the typical CV pattern of the OPFMCC-PVA-$LiClO_4$ film at the scan rate of 10 mV s^{-1}. It was revealed that the electrochemical stability window potential of S5 film around 1.9 V.

Table 4. The parameters of ionic conductivity for composite polymer of OPF MCC

Sample	Thickness, $\times 10^{-3}$ (cm)	$R_b \times 10^3$ (Ω cm^2)	Conductivity,σ (S cm^{-1})
S1 (OPF MCC: PVA: 0 % $LiClO_4$)	67.5 ± 0.71	309.7 ± 0.85	1.07×10^{-6}
S2 (OPF MCC: PVA: 5 % $LiClO_4$)	42.5 ± 0.71	7.3 ± 0.66	1.21×10^{-5}
S3 (OPF MCC: PVA: 10 % $LiClO_4$)	81.0 ± 4.24	10.4 ± 0.67	3.83×10^{-5}
S4 (OPF MCC: PVA: 15 % $LiClO_4$)	72.0 ± 1.41	5.3 ± 0.43	6.63×10^{-5}
S5 (OPF MCC: PVA: 20 % $LiClO_4$)	64.0 ± 0.05	1.7 ± 0.035	1.88×10^{-4}
Modified cellulose-PVA:20 % $LiClO_4$ [43]	NA	NA	8.03 x 10^{-6}

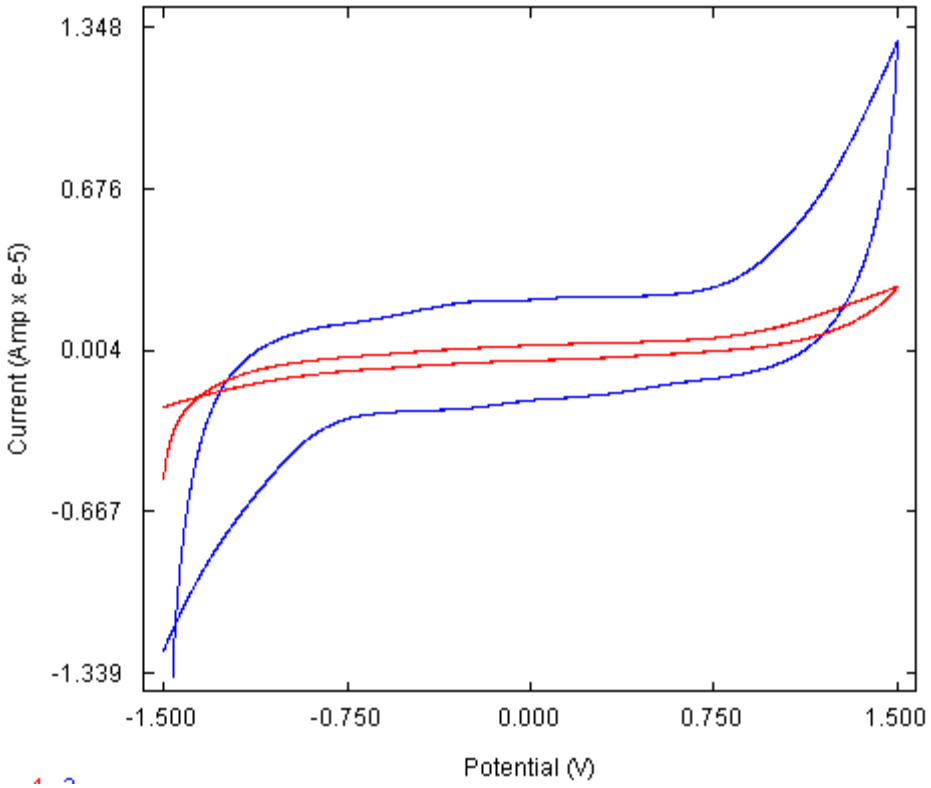

Figure 9. The overlay of cyclic voltammetry curves of the S1 (red) and S5(blue) polymer electrolyte film

4. CONCLUSION

MCC from OPF pulp has been successfully isolated using acid hydrolysis treatment. It was revealed that the isolated OPFMCC was cellulose type I polymorph and it consisted of higher degree of crystallinity with low molecular weight than the α-cellulose. Different compositions of OPFMCC-PVA-$LiClO_4$ polymer electrolyte have been successfully prepared *via* solution casting technique. The ionic conductivity of the prepared film was increased by increasing the salt concentration. A maximum conductivity was found to be 1.88×10^{-4} S cm^{-1} for S5 (OPFMCC-PVA-20 % $LiClO_4$) with electrochemical stability window potential around 1.9 V. The highest ionic conductivity of the cellulose-based polymer electrolyte is suit well for their further applications especially in the performance of Li ion batteries.

ACKNOWLEDGEMENT
The authors are grateful for their financial support of this research from Universiti Sains Malaysia through USM Short Term Grant- 304/PKIMIA/6313216.

References

1. P. Tamilselvi, M. Hema, *Physica* B. 437 (2014) 53-57.
2. F. Croce, G.B. Appetecchi, L. Persi, B. Scrosati, *Nature* 394 (1998) 456-458.
3. R. Premila, S. Rajendran, *Adv. Eng. Appl. Sci.: An Int. J.* 5 (2015) 32-33.
4. J. Tang, R. Muchakayala, S. Song, M. Wang, K.N. Kumar, *Polym. Test*. 50 (2016) 247-254.
5. Y.T. Jia, J. Gong, X.H. Gu, H.Y. Kim, J. Dong, X.Y. Shen, *Carbohyd. Polym*. 67 (2007) 403-409.
6. S.G. Rathod, R.F. Bhajantri, V. Ravindrachary, P.K. Pujari, G.K. Nagaraja, J. Naik, V. Hebbar, H. Chandrappa, B. *Mater. Sci.* 38 (2015) 1213-1221.
7. D.H. Krassig, Structure of cellulose and its relation to properties of cellulose fibers, in: J.F. Kennedy (Ed), Cellulose and its derivatives. John Wiley and Sons, Chichester, 1985.
8. A.N. Fernandes, L.H. Thomas, C.M. Altaner, P. Callow, V.T. Forsyth, D.C. Apperley, C.J. Kennedy, M.C. Jarvis, *Proc. Natl. Acad. Sci*. 108 (2011) 1195-1203.
9. J.F. Revol, D.A.I. Goring, *J. Appl. Polym. Sci*. 26 (1981) 1275-1282.
10. E. Kontturi, T. Tammelin, M. Österberg, *Chem. Soc. Rev.* 35 (2006) 1287-1304.
11. M.K. Mohamad Haafiz, S.J. Eichhorn, A. Hassan, M. Jawaid, *Carbohyd. Polym*. 93 (2013) 628-34.
12. Y.P. Chauhan, R.S. Sapkal, V.S. Sapkal, G.S. Zamre, *Int. J. Chem. Sci*. 7 (2009) 681-688.
13. D. Trache, M.H Hussin, C.T.H. Chuin, S. Sabar, M.R.N. Fazita, O.F.A. Taiwo, T.M. Hassan, M.K.M. Hafiz, *Int. J. Biol. Macromol*. 93 (2016) 789-804.
14. D. Trache, A. Donnot, K. Khimeche, R. Benelmir, N. Brosse, *Carbohyd. Polym*. 104 (2014) 223-230.
15. B. Chamsai, P. Sriamornsak, *Powder Technol*. 233 (2013) 278-285.
16. M. El-Sakhawy, M.L. Hassan, *Carbohyd. Polym.* 67 (2007) 1-10.
17. A.M.N. Galal, A.M.H. Fatma, K.E. Ali, M.K. Jihan, H.S.M. Sahar, *J. Am. Sci*. 6 (2010) 226-231.
18. M.H. Hussin, N.A. Pohan, Z.N. Garba, M.J. Kassim, A.A. Rahim, N. Brosse, M.Yemloul, M.R.N. Fazita, M.K.M. Haafiz, *Int. J. Biol. Macromol*. 92 (2016) 11-19.
19. M.W. Zahari, O.A. Hassan, H.K. Wong, J.B. Liang, *Asian Austral. J. Anim*. 16 (2003) 625-634.
20. M.H. Hussin, A.A. Rahim, M.N.M. Ibrahim, N. Brosse, *Ind. Crop Prod*. 49 (2013) 23-32.

21. I. Dahlan, *Asian Austral. J. Anim*. 13 (2000) 300-303.
22. H. Kawamoto, W.Z. Mohamed, N.I.M. Sukur, M.M. Ali, Y. Islam, S. Oshio, *Jarq-Jpn. Agr. Res.*Q. 35 (2001) 195-200.
23. B. Salamatinia, A.H. Kamaruddin, A.Z. Abdullah, *Chem. Eng. J.* 156 (2010) 141-145.
24. S. Sabiha-Hanim, M.A.M. Noor, A. Rosma, *Bioresource Technol*. 102 (2011) 1234-1239.
25. C.S. Goh, K.T. Lee, S. Bhatia, *Bioresource Technol*. 101 (2010) 7362-7367.
26. M.H. Hussin, A.A. Rahim, M.N.M. Ibrahim, N. Brosse, *Mater. Chem. Phys*. 163 (2015) 201-212.
27. R. El Hage, N. Brosse, L. Chrusciel, C. Sanchez, P. Sannigrahi, A. Ragauskas, *Polym. Degrad. Stabil.* 94 (2009) 1632-1638.
28. Y.P. Timilsena, C.J. Abeywickrama, S.K. Rakshit, N. Brosse, *Bioresource Technol*. 135 (2013) 82-88.
29. Y.N. Sudhakar, M. Selvakumar, *Electrochim. Acta*, 78 (2012) 398-405.
30. C.P. Azubuike, A.O. Okhamafe, *Int. J. Recycl. Org. Waste Agric*. 1 (2012) 1-7.
31. M.B. Foston, C.A. Hubbell, A.J. Ragauskas, *Materials*, 4 (2011) 1985-2002.
32. R.G. Zhbankov, Infrared spectra of cellulose and its derivatives, Consultants Bureau, Pleum Publishing Corporation, New York, 1966.
33. S.M. Rosa, N. Rehman, M.I.G. de Miranda, S.M. Nachtigall, C.I. Bica, *Carbohyd. Polym*. 87 (2012) 1131-1138.
34. N. Johar, I. Ahmad, A. Dufresne, *Ind. Crop. Prod*. 37 (2012) 93-99.
35. R.D. Kalita, Y. Nath, M.E. Ochubiojo, A.K. Buragohain, *Colloid Surface* B, 108 (2013) 85-89.
36. R. Li, J. Fei, Y. Cai, Y. Li, J. Feng, J. Yao, *Carbohyd. Polym*. 76 (2009) 94-99.
37. F. Fahma, S. Iwamoto, N. Hori, T. Iwata, A. Takemura, *Cellulose*, 17 (2010) 977-985.
38. A. Alemdar, M. Sain, *Bioresource Technol*. 99 (2008) 1664-1671.
39. P.T. Larsson, U. Westermark, T. Iversen, *Carbohyd. Res*. 278 (1995) 339-343.
40. R.H. Newman, J.A. Hemmingson, *Cellulose*, 2 (1995) 95-110.
41. P.K. Gupta, V. Uniyal, S. Naithani, *Carbohyd. Polym*. 94 (2013) 843-849.
42. S. Brunauer, P. H. Emmett, E. Teller, *J. Am. Chem. Soc*. 60 (1938) 309-319.
43. S.G. Rathod, R.F. Bhajantri, V. Ravindrachary, P.K. Pujari, G.K. Nagaraja, J. Naik, V.A. Hebbar, H. Chandrappa, *Bull. Mater. Sci.* 38 (2015) 1213–1221.